Trans. JSASS Aerospace Tech. Japan
Vol. 16, No. 3, pp. 285-290, 2018
DOI: 10.2322/tastj.16.285

Design of a MEMS-Mirror-based Laser Pointing Control System of Optical Transponder for Micro-satellites

By Toshinori KUWAHARA,[1)] Shinya FUJITA,[1)] Yuji SATO,[1)] Shota SUZUKI,[1)] and Lena OKAJIMA[2)]

[1)]*Department of Aerospace Engineering, Tohoku University, Sendai, Japan*
[2)]*ALE Co., Ltd., Tokyo, Japan*

(Received June 30th, 2017)

Optical communication technologies are regarded as an important breakthrough for future satellite communications. Tohoku University has been developing Adjustable beam angle Small Optical TrAnsponder (ASOTA) for micro-satellites. The design concept of ASOTA is miniaturization and low power consumption. It is necessary for space optical communication to direct the laser to the ground station with a high precision. This research describes the development of a MEMS-Mirror-based Fine Pointing Mechanism (FPM). The MEMS mirror is suitable for micro-satellites because it is smaller and consumes less power than 2-axis gimbal mechanisms. FPM is a feedback control system consisting of a MEMS mirror and a Quadrant Detector. The characteristics and mathematical model of each device are described. Then numerical simulation and ground evaluation results of FPM with a simple optical system are summarized.

Key Words: Optical Communication, Laser Tracking, MEMS Mirror, Micro-satellite, Closed Loop Control

Nomenclature

d	:	distance
e	:	error
f	:	intensity distribution function
G	:	transfer function
I	:	current
K	:	control gain
ND	:	normalized distance
R	:	radius
s	:	complex variable
T	:	control cycle
V	:	voltage
x	:	x-axis
X	:	normalized coordinate in x direction
y	:	y-axis
Y	:	normalized coordinate in y direction
z	:	z-axis
η	:	light receiving sensitivity
θ	:	angle

Subscripts

A	:	light receiving surface A of QD
B	:	light receiving surface B of QD
C	:	light receiving surface C of QD
D	:	light receiving surface D of QD
mirror	:	MEMS mirror
offset	:	offset
PSD	:	position sensitive detector
QD	:	quadrant detector
Ref	:	reference
sim	:	simulation

1. Introduction

Recently, due to the dramatical improvement of on-board observation instruments, as well as the increase of communication and broadcasting satellite services, there is a significant demand on high-speed satellite-to-ground communication capabilities. Though higher frequency band such as Ka-band is recently being utilized for high-speed radio wave communications, optical communication technologies are regarded as indispensable to achieve much higher data rate to satisfy future demands on data transmission.[1)] Optical communication has advantages in efficiency of energy usage due to its narrow beamwidth, miniaturization of the antenna, and higher security in terms of interception.[2)] The number of micro-satellites will continue to increase, but the resource of radio wave frequency band is limited.[3)] Space optical communication avoids this congestion. Hence it is necessary to develop an optical transponder for micro-satellites. Table 1 shows the previous studies. SOTA developed by NICT successfully downlinked by laser with 15.7W, which is less than 1/10 of LUCE, which is the world's first transponder for LEO-ground optical communication.[4,5)] VSOTA developed by NICT and Tohoku University is scheduled to be installed in micro-satellite RISESAT, and its power consumption is 10W or less. [6,7)]

One of the technical problems is the laser pointing control between optical antennas.[8)] In order to solve this problem, the laser tracking system is used for most optical transponders. SOTA had a 2-stage laser tracking system with a 2-axis gimbal and a mirror.[9)] However, the scale of the device was still large for micro-satellite or CubeSat. Though VSOTA is extremely compact and has a high mountabiliy. it does not have a laser tracking system, and hence the laser divergence angel increases resulting in lower data rate.

Tohoku University is developing ASOTA. The design concept of ASOTA is the miniaturization and low power consumption. FPM of the ASOTA's laser tracking system using electrostatic drive type MEMS mirror reduces the scale and power consumption of the device. This will make it possible to install a high-speed optical transponder on satellites with limited resources. It feedbacks the direction of arrival of the beacon light from the ground station acquired at the QD to the MEMS mirror, and performs directional control of the downlink laser (Fig. 1.).

Table 1. Specification of optical transponder for micro-satellites.[10)]

Items	SOTA	VSOTA	ASOTA
Data rate [Mbps]	10	0.1	10
Mass [kg]	5.9	1	1.5
Power [W]	15.7	10	8
Tracking system	2-axis gimbal and mirror	N/A	MEMS mirror

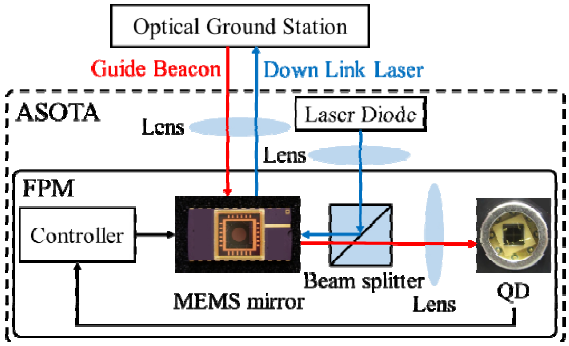

Fig. 1. Block diagram of FPM.

2. Performance Requirements

The guide beacon from the optical ground station and the downlink laser from ASOTA are reflected by a single MEMS mirror. By appropriately controlling the MEMS mirror, the spot of the guide beacon coincides with the center of the QD. In this state, the transmit beam is automatically directed to the ground station by the optical design of ASOTA. Therefore, direction control of the downlink laser is the same as irradiating the center of the QD with the beacon light spot. The role of FPM is to lower the laser pointing error that cannot be eliminated by satellite attitude control below the divergence angle. Considering the application environment of ASOTA, the center of the light spot must be within the range of 3.75μm from the center of the QD. In addition, the MEMS mirror needs to move ±3deg 2-dimensionally. If the optical ground station being developed by Tohoku University irradiates beacon, the QD must detect 570-850pW of light.

3. Characteristic Measurement

3.1. MEMS mirror

Characteristics of the MEMS mirror were measured. The input of the MEMS mirror is voltage and the output is angle. The principle of characteristic measurement is shown in Fig. 2. The voltage-applied MEMS mirror is irradiated with a laser, and the position of the reflected light is measured by 1-dimensional Position Sensitive Detector (PSD) and TransImpedance Amplifier (TIA). The drive angle of the MEMS mirror is calculated by Eq. (1).

$$\theta_{mirror} = \frac{1}{2}\tan^{-1}\left(\frac{x_{PSD}}{d_{PSD}}\right) \tag{1}$$

When measuring static characteristics, the constant voltage is applied to the MEMS mirror. The frequency characteristic is measured by the sinusoidal sweep method.[11)] The gain and phase at a certain frequency are calculated from the response of the drive angle to the applied sinusoidal voltage. Complex frequency response is calculated from them, and the MEMS mirror is system-identified using MATLAB/Simulink System Identification Toolbox. Measurements are made in each direction because the MEMS mirror is driven 2-dimensionally (Fig. 3.).

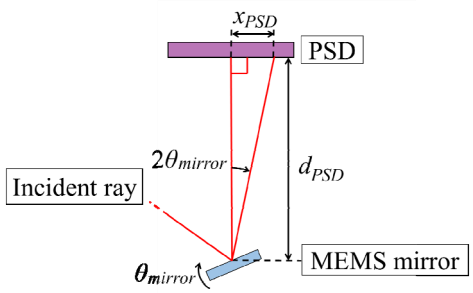

Fig. 2. Measurement principle of MEMS mirror drive angle.

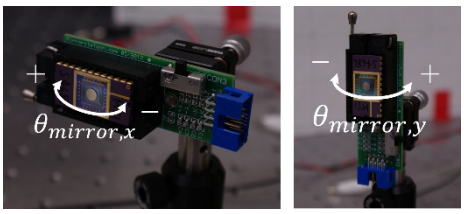

Fig. 3. Measurement direction of MEMS mirror (left: around x_{mirror} axis, right: around y_{mirror} axis).

The measurement results of static characteristics are shown in Fig. 4. The input voltage and the drive angle are proportional in each direction. It can be confirmed that it satisfies required performance ±3deg by using a high voltage. The Bode diagram is shown in Fig. 5. The MEMS mirror has a frequency band of 300Hz. Figure 5 also shows the results of system identification. The conformance rate of the estimation is 84%. The transfer function obtained by system identification is shown in Eq. (2) and (3).

$$G_{mirror,x} = \frac{2.394\times10^5}{s^2+182.1s+7.927\times10^6} \tag{2}$$

$$G_{mirror,y} = \frac{2.453\times10^5}{s^2+150.6s+7.847\times10^6} \tag{3}$$

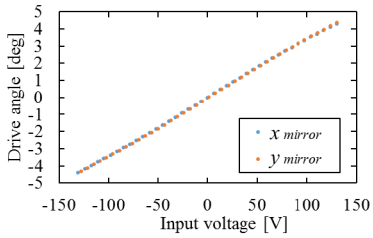

Fig. 4. Relation between MEMS mirror input voltage and drive angle.

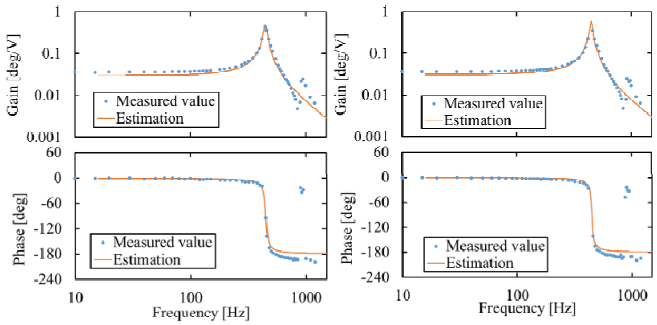

Fig. 5. Bode plot of MEMS mirror (left: x_{mirror} direction, right: y_{mirror} direction.)

3.2. QD driver

The definition of the QD light receiving surface is shown in Fig. 6. From the output current of each light receiving surface, the normalized coordinates of the spot can be obtained by following equations.

$$X_{QD} = \frac{\left(I_{QD,B} + I_{QD,C}\right) - \left(I_{QD,A} + I_{QD,D}\right)}{I_{QD,A} + I_{QD,B} + I_{QD,C} + I_{QD,D}} \tag{4}$$

$$Y_{QD} = \frac{\left(I_{QD,A} + I_{QD,B}\right) - \left(I_{QD,C} + I_{QD,D}\right)}{I_{QD,A} + I_{QD,B} + I_{QD,C} + I_{QD,D}} \tag{5}$$

where

$$I_{QD,A} = \eta \int_{d_{QD}/2}^{\sqrt{R_{QD}^2 - x_{QD}^2}} \int_{-\sqrt{R_{QD}^2 - d_{QD}^2/4}}^{-d_{QD}/2} f\left(x_{QD}, y_{QD}\right) dx_{QD} dy_{QD} \tag{6}$$

$$I_{QD,B} = \eta \int_{d_{QD}/2}^{\sqrt{R_{QD}^2 - x_{QD}^2}} \int_{d_{QD}/2}^{\sqrt{R_{QD}^2 - d_{QD}^2/4}} f\left(x_{QD}, y_{QD}\right) dx_{QD} dy_{QD} \tag{7}$$

$$I_{QD,C} = \eta \int_{-\sqrt{R_{QD}^2 - x_{QD}^2}}^{-d_{QD}/2} \int_{d_{QD}/2}^{\sqrt{R_{QD}^2 - d_{QD}^2/4}} f\left(x_{QD}, y_{QD}\right) dx_{QD} dy_{QD} \tag{8}$$

$$I_{QD,D} = \eta \int_{-\sqrt{R_{QD}^2 - x_{QD}^2}}^{-d_{QD}/2} \int_{-\sqrt{R_{QD}^2 - d_{QD}^2/4}}^{-d_{QD}/2} f\left(x_{QD}, y_{QD}\right) dx_{QD} dy_{QD} \tag{9}$$

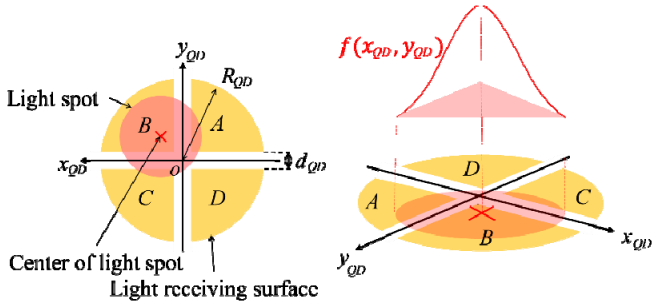

Fig. 6. Conceptual scheme of QD.

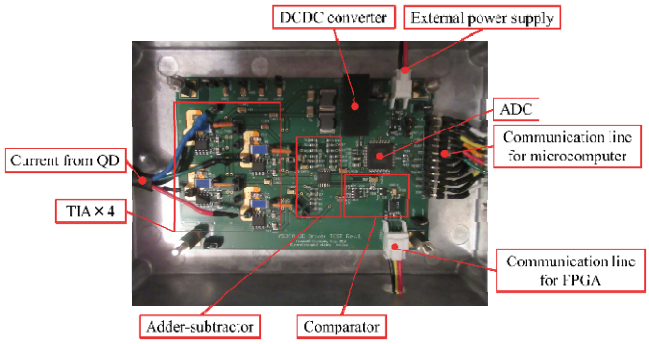

Fig. 7. Overview of QD driver.

QD driver to process the output of QD was designed (Fig. 7.). It consists of high sensitivity TIA, addition/subtraction circuit and AD converter. The relationship between the spot position and the normalized coordinates was measured to confirm that all of them operate correctly. For the experiment, Gaussian beam which simulated the environment of ASOTA was used (diameter: 500μm, power: 570pW). The spot position is moved by the translation stages and the normalized coordinates are measured. The theoretical values of them are calculated using numerical integration of MATLAB/Simulink. The spot position is shown in Fig. 8, and the results are shown in Fig. 9. As a result of the comparison, it was confirmed that these values coincided and QD driver operates correctly.

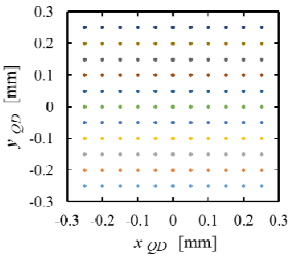

Fig. 8. Light spot center position of QD driver test.

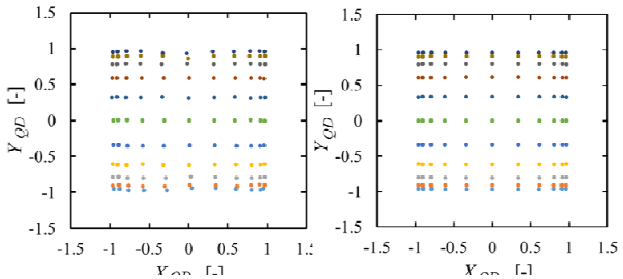

Fig. 9. Normalized coordinates (left: result, right: theoretical plot).

Next, the frequency characteristic of the high sensitivity TIA is measured. It is measured by step input transient response method. The time constant is calculated from the output of the TIA when the laser is turned on. The gain is not considered because it is determined by the feedback resistance. The step responses are shown in Fig. 10. TIA is regarded as a second-order lag element from this result. System identification is performed based on the overshoot and the cycle of damped oscillation. The transfer functions of each element obtained by system identification are shown in the following equations. Figure 10 also shows the step responses of Eqs. (10)-(13) calculated by MATLAB/Simulink.

$$G_A = \frac{1.463\times10^5}{s^2+281.5s+1.463\times10^5} \tag{10}$$

$$G_B = \frac{1.778\times10^5}{s^2+248.3s+1.778\times10^5} \tag{11}$$

$$G_C = \frac{1.681\times10^5}{s^2+237.2s+1.681\times10^5} \tag{12}$$

$$G_D = \frac{1.225\times10^5}{s^2+119.0s+1.225\times10^5} \tag{13}$$

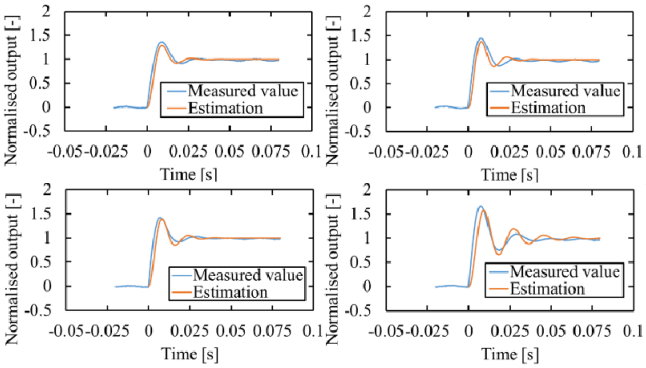

Fig. 10. Step response of TIA (upper left: surface A, upper right: surface B, lower left: surface C, lower right: surface D).

4. Ground Evaluation System

4.1. Configuration

For ground evaluation, FPM was constructed with the MEMS mirror and the QD (Fig. 11). QD driver processes the output current of the QD on which the light spot is incident. The microcomputer on the control board calculates normalized coordinates from the output of the QD driver with digital low-pass filter. Then, the microcomputer calculates the input voltage to the MEMS mirror according to the control law described later. Finally, the voltage is applied to the MEMS mirror by the amplifier, and the drive angle is changed. The position of the spot irradiated to the QD is controlled to the center of it by changing the direction of the reflected light. The normalized coordinates of the spot and voltage of MEMS mirror are recorded in PC.

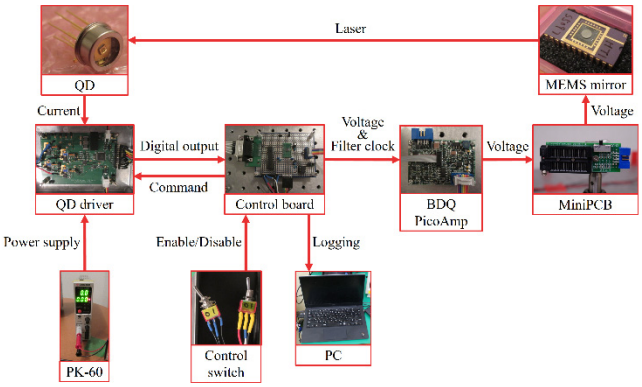

Fig. 11. System configuration of FPM for ground evaluation.

4.2. Optical system

At present, the ASOTA optical system is under development. Therefore, a simple optical system constructed on an optical bench is used in this research (Fig. 12). This consists of a MEMS mirror tilted by 45deg and a QD tilted by 90deg. The distance from the MEMS mirror to the QD is 100mm based on the length of 1U CubeSat. The disturbance is the parallel movement of the collimator. The FPM corrects this deviation of the spot by a control law described later.

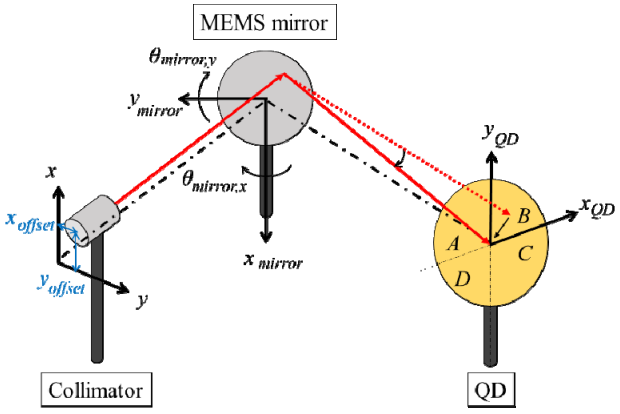

Fig. 12. Simple optical system for ground evaluation.

4.3. Control algorithm

The block diagram of FPM is shown in Fig. 13. The position of spot on the QD was separated in horizontal and vertical direction, and the controllers are applied to each loop. The two control loops integrated in the optical system block. The controlled object is a series of blocks from MEMS mirror to QD. The controlling variable is the input voltage to the MEMS mirror. The controlled variable is the normalized coordinates of the spot. Originally, it should be the position of the spot x_{QD}, y_{QD}, normalized coordinates can be substituted by using the correspondence relationship of them. The purpose of FPM is to keep the spot at the center of the QD. Therefore, the desired value is $(x_{QD}, y_{QD}) = (0,0)$. When replaced with normalized coordinates, it is $(X_{Ref}, Y_{Ref}) = (0,0)$. The disturbance input to the optical system is the pointing error of the satellite in the case of

ASOTA, which corresponds to the parallel movement of the collimator in the case of a simple optical system. If disturbance does not occur, the spot is in the center of the QD without driving the MEMS mirror. FPM eliminates steady-state error only when disturbance occurs. For this reason, integral control is applied to FPM in this paper. Trapezoidal numerical integration is applied to the calculation. The control cycle is 0.3s.

$$V_{mirror,x,y}(t) = K_{x,y}\int_0^t e_{x,y}(\tau)d\tau \approx K_{x,y}\sum_{k=1}^{n}\frac{e_k + e_{k-1}}{2}T \tag{14}$$

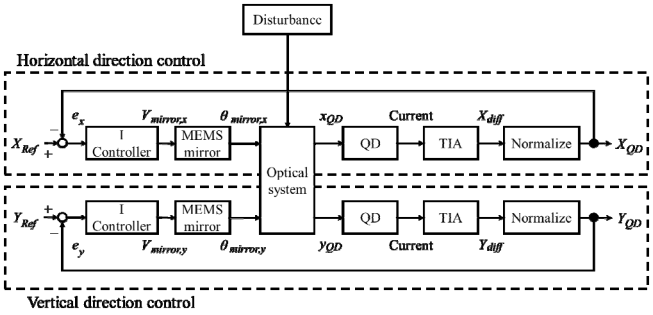

Fig. 13. Control loop of FPM.

5. Simulation

In order to verify the effectiveness of the control law, FPM simulation was performed on MATLAB Simulink. Obtained transfer functions Eq. (2), (3) and (10)-(13) are applied to MEMS mirror and TIA blocks. Eq. (6)-(9) are applied to QD block. Eq. (14) is applied to controller block. Ray tracing of reflected light is calculated in optical system block. To calculate the attitude of the MEMS mirror, Rodrigues' rotation formula is used.[12] The simulation conditions are shown in Table 2. A part of the simulation results is shown in Fig. 14. Simulation results confirmed that the proposed closed loop control functions stably.

Table 2. Simulation conditions.

Items	Values
Time [s]	11 (FPM become effective 1s later.)
Laser power [pW]	570
Spot diameter [μm]	500
(x_{offset}, y_{offset}) [mm]	$(-0.25,0.00),(0.00,0.25),$ $(0.18,-0.18)$
(K_x, K_y) [-]	$(-0.01,0.01),(-0.015,0.015),$ $(-0.02,0.02),(-0.03,0.03)$

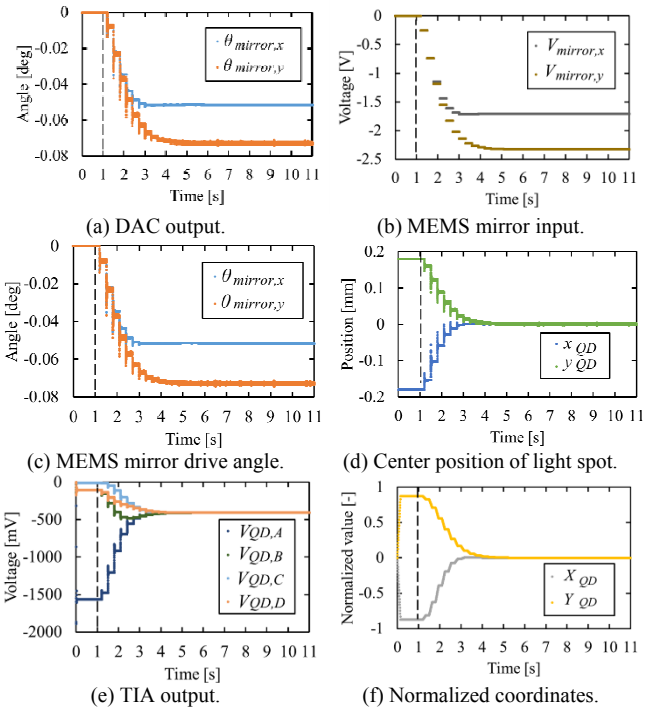

(a) DAC output. (b) MEMS mirror input.
(c) MEMS mirror drive angle. (d) Center position of light spot.
(e) TIA output. (f) Normalized coordinates.

Fig. 14. Results of FPM simulation $(x_{offset}, y_{offset}) = (0.18,-0.18)$, $(K_x, K_y) = (-0.015,0.015)$.

6. Ground Test

An experiment was performed to verify that FPM in real space is feasible (Fig. 15). The experimental conditions are the same as the simulation shown in Table 2. The normalized distance shown in Eq. (15) is defined in order to measure the pointing accuracy.

$$ND = \sqrt{X_{QD}^2 + Y_{QD}^2} \tag{15}$$

When the spot of light is within the range of 3.75μm from the center of QD, *ND* is 0.0262 or less. FPM must fulfill this condition. A part of the ground evaluation results is shown in Fig. 16. The validity of the experiment can be confirmed from the comparison with the simulation results. The normalized distance converges to 0.0262 or less, and the developed FPM satisfies the required orientation accuracy. The time it takes for the error to settle is shown in Fig. 17. Increasing the gain improves quick response, but too large will increase settling time due to overshoot. The power consumption of the FPM under control is 0.55W, which is lower than the conventional model.

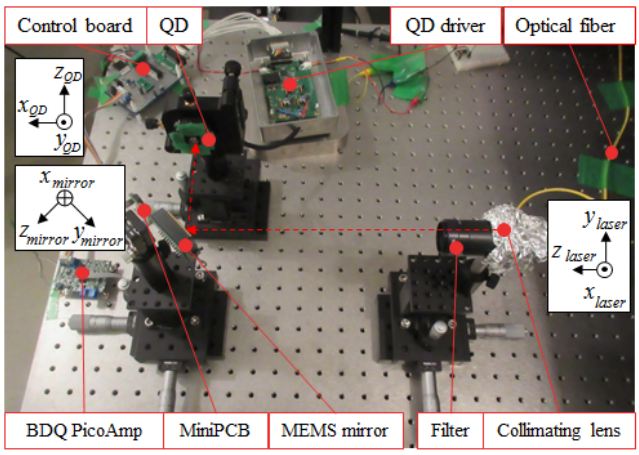

Fig. 15. Experimental system for FPM with simple optical system.

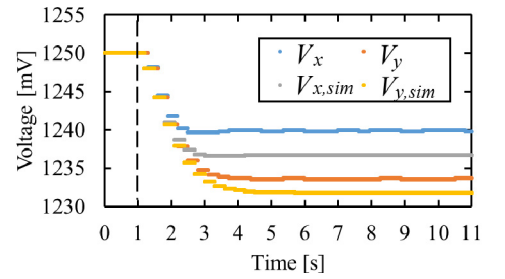

(a) DAC output.

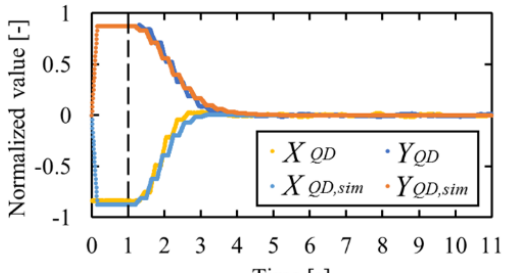

(b) Normalized coordinates.

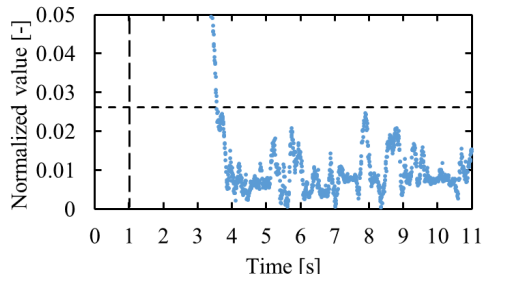

(c) Normalized distance.

Fig. 16. Result of ground test $(x_{offset}, y_{offset}) = (0.18, -0.18)$, $(K_x, K_y) = (-0.015, 0.015)$.

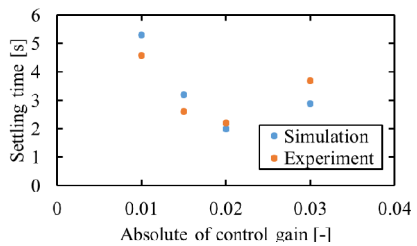

Fig. 17. Settling time receiving effect of control gain.

7. Conclusion

A MEMS-Mirror-based FPM was developed and a laser tracking control law of FPM was proposed. The effectiveness of the control law was demonstrated by simulation using the estimated model. The experimental environment of the laser pointing control in real space was realized using the simple optical system and FPM. Finally, the pointing accuracy and power consumption were measured through experiments and it was shown that the developed FPM is a suitable laser tracking system for ASOTA.

Acknowledgments

The authors thank National Institute of Information and Communication Technology (NICT) for technical support for this research.

References

1) Kadowaki, N., Toyoshima, M., Miura, A., Yamamoto, S., Takahashi, T., Yoshimura, N., Tsuji, H., Takizawa, K., Takayama, Y., and Munemasa, Y.: Recent Trends of Satellite Communication Technologies Applied to New Frontiers, *IEICE Trans. Commun. (Japanese Edition)*, **J97-B** (2014), pp. 979-991.
2) Yamada, S., Fukakura, E., Tabata, M., and Shiratama, K.: Communications Technologies Supporting Satellite Communications, *NEC Technical Journal*, **6** (2011), pp. 96-100.
3) About International Adjustment of Satellite Frequency, http://www.tele.soumu.go.jp/resource/j/freq/process/kokata.pdf (in Japanese) (accessed March 23, 2017).
4) Shiratama, K., Aizono, M., Kumagai, T., Ikebe, K., Mase, I., Jono, T., Takayama, Y., Ohinata, K., Kura, N., Koyama, Y., Arai, K., and Abe, J.: On-orbit test results of Laser Utilizing Communications Equipment (LUCE) on Optical Inter-orbit Communications Engineering Test Satellite (OICETS), *IEICE Technical Report (SANE)*, **106** (2006), pp. 63-68.
5) Optical Satellite Communication with 1.5 micron Light between LEO Satellite and Ground, NICT, https://www.nict.go.jp/press/2015/06/03-2.html (in Japanese) (accessed March 23, 2017).
6) Kunimori, H., Takenaka, H., Fuse, T., Gotoh, T., Kubooka, T., Toyoshima, M., Yoshida, K., and Kuwahara, T.: VSOTA:Optical Communication Terminal on a small satellite HODOYOSHI-2, *IEICE Technical Report (SANE)*, **112** (2012), pp. 99-104.
7) Kuwahara T., Yoshida, K., et al.: Satellite-to-Ground Optical Communication System on Low Earth Orbit Micro-satellite RISESAT, *Proc. 2012 IEEE/SCIE Symposium on System Integration*, (2012), pp.939-944.
8) Takayama, Y.: Current situation and future trend of space optical communication, *The Society of Japanese Aerospace Companies,* **732** (2014), pp. 4-10.
9) Koyama, Y., Toyoshima, M., Takayama, Y., Takenaka, H., Shiratama, K., Mase, I., and Kawamoto, O.: SOTA:Small Optical Transponder for Micro-Satellite, IEEE ICSOS 2011, pp. 97-101.
10) Munemasa, Y., Koyama, Y., Akioka, M., and Toyoshima, M.: A Feasibility Study of an Optical Antenna Measuring on LEO Using Small Optical TrAnsponder (SOTA), *IEICE Technical Report (SAT)*, **115** (2015), pp. 31-34.
11) Adachi, S.: *System Identification Basics*, Tokyo Denki University Press, 2009.
12) Uchiyama, M. and Nakamura, Y.: *Robot motion*, Iwanami Shoten Publishers, 2004.